Electronic Supplementary Information for

From Deep Blue to Green Emitting and Ultralong Fluorescent Copper(I) Halide Complexes Containing Dimethylthiophene Diphosphine and PPh_3 Ligands

Qiong Wei, Rui Zhang, Li Liu*, Xin-Xin Zhong*, Lei Wang*, Guang Hua Li, Fa-Bao Li, Khalid A. Alamry, Yi Zhao

Contents

Table S6. Computed excitation states for complex **2** in CH_2Cl_2.

Table S7. Computed excitation states for complex **3** in CH_2Cl_2.

Experimental Details

1. NMR Experiments

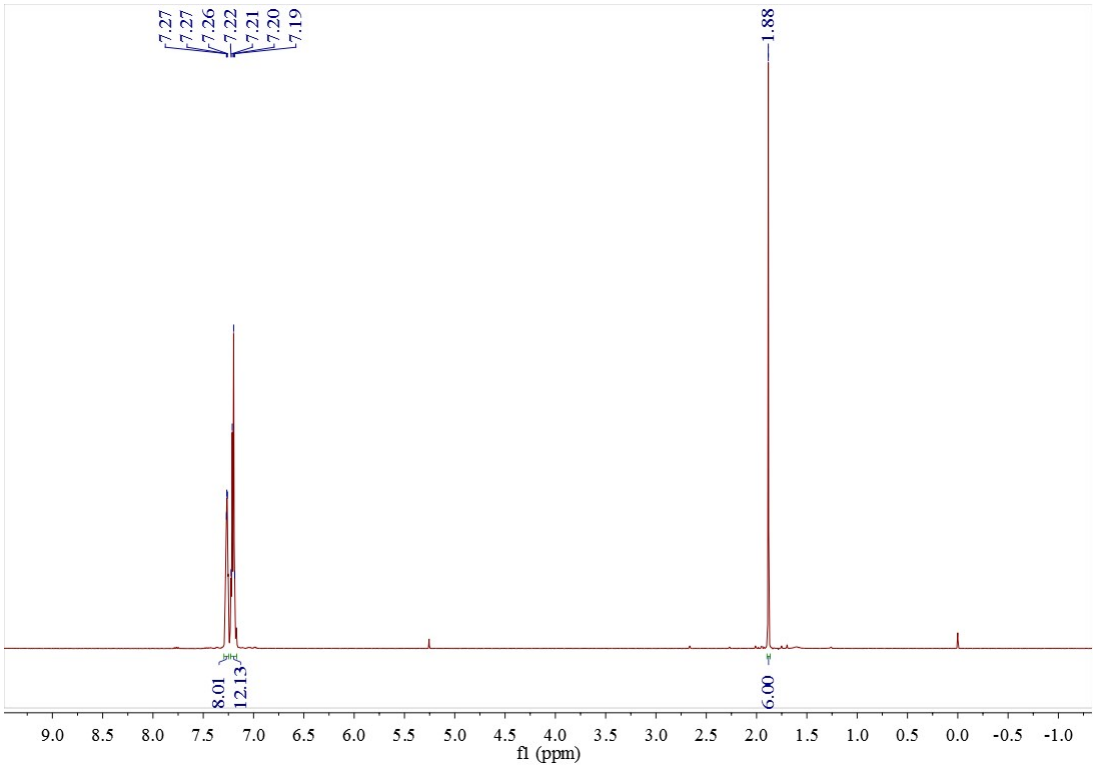

Fig. S1 ^{1}H NMR spectrum of **dpmt** in $CDCl_3$.

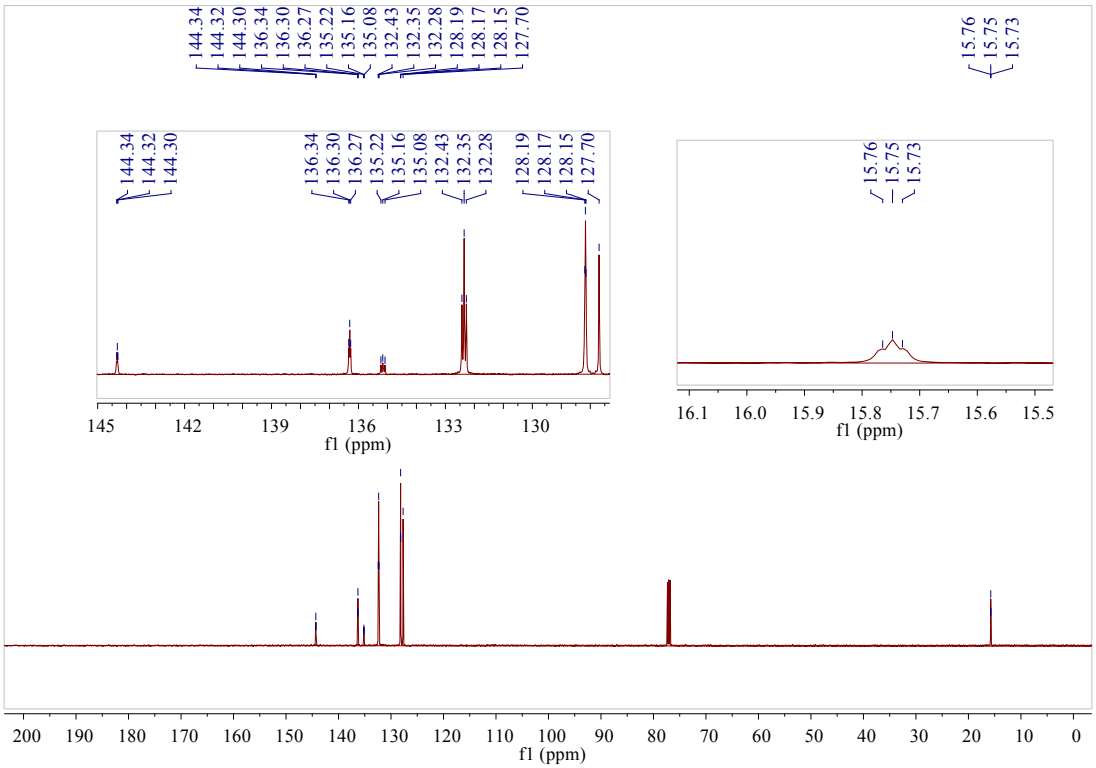

Fig. S2 ^{13}C NMR spectrum of **dpmt** in $CDCl_3$.

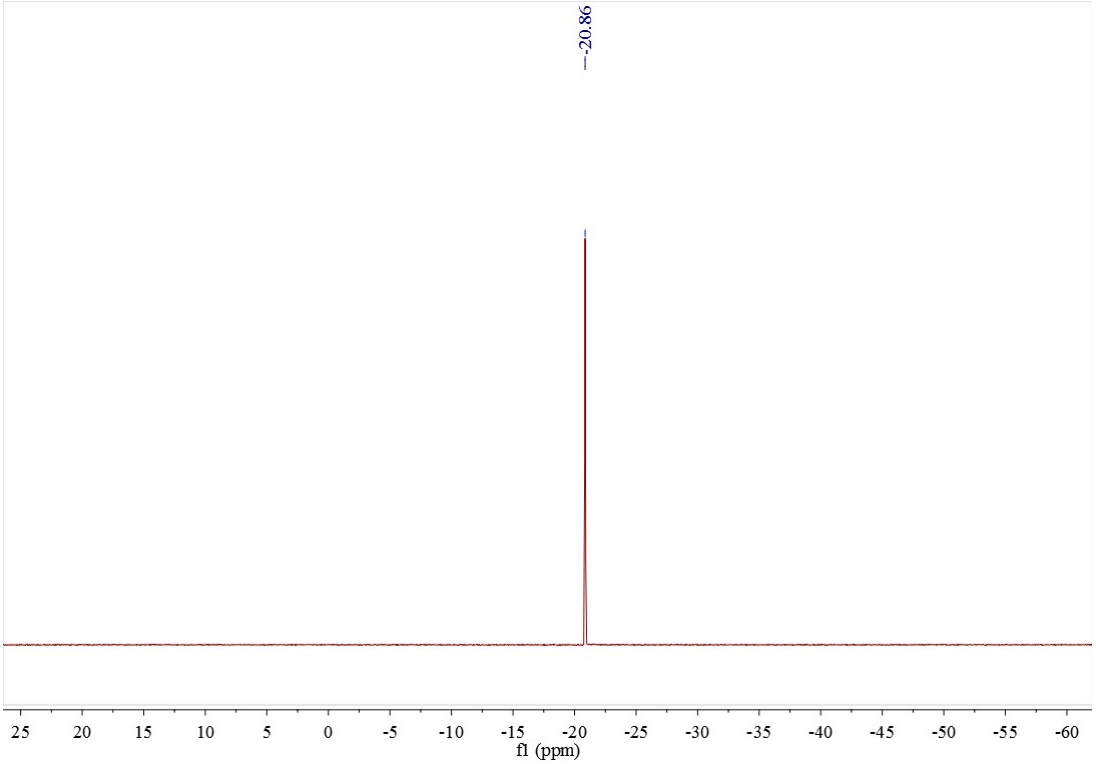

Fig. S3 ^{31}P NMR spectrum of **dpmt** in $CDCl_3$.

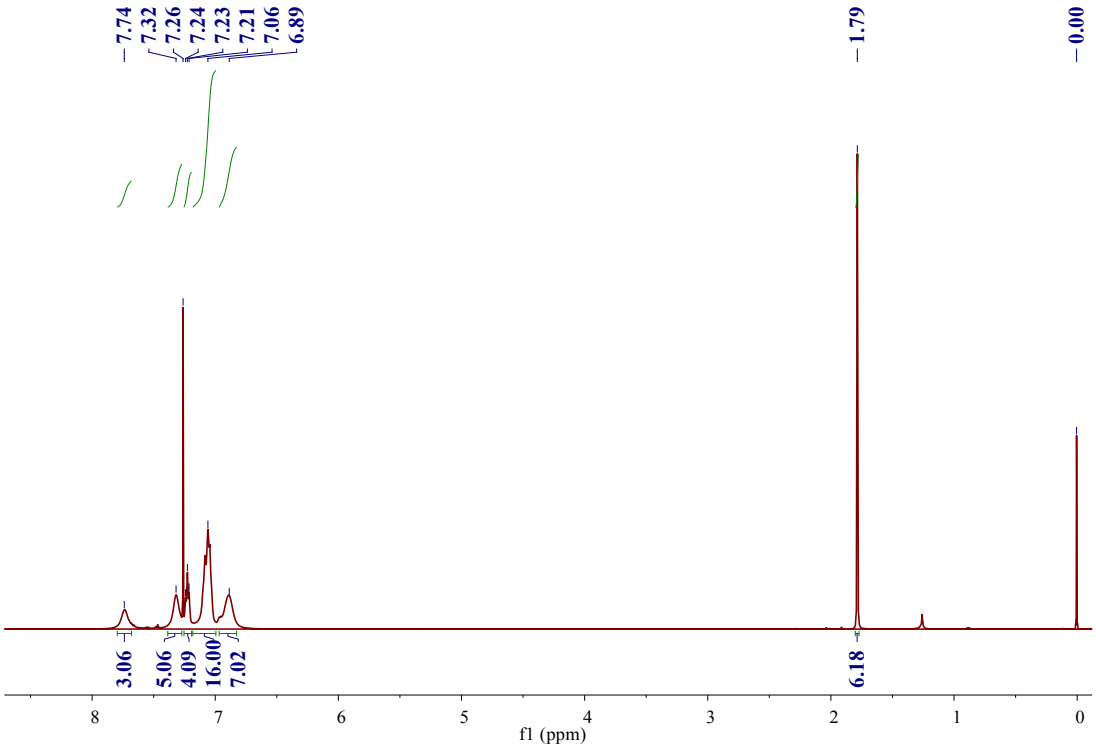

Fig. S4. ^{1}H NMR spectrum of **1** in $CDCl_3$.

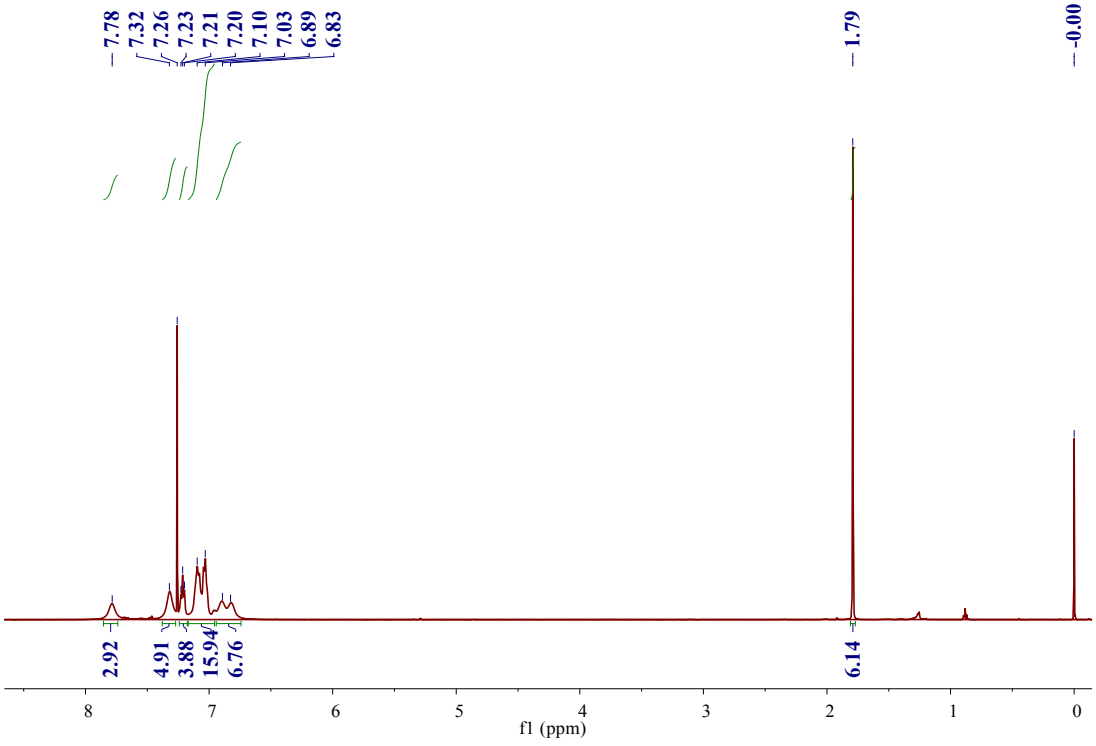

Fig. S5. ^{1}H NMR spectrum of **2** in $CDCl_3$.

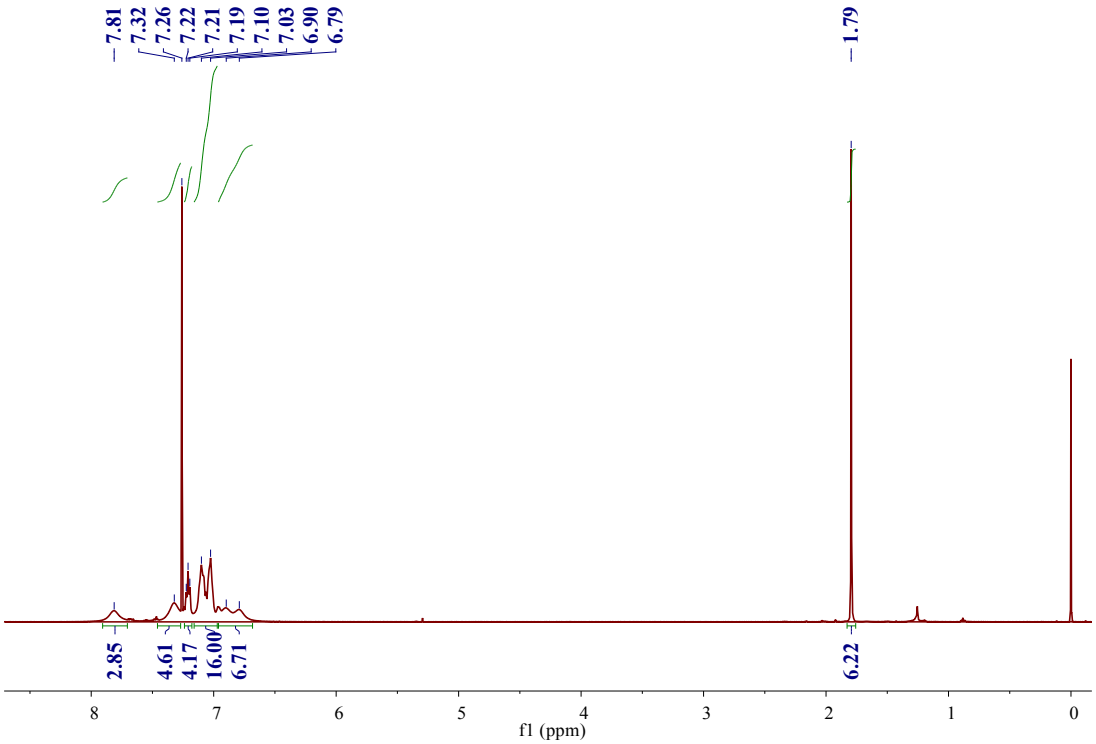

Fig. S6. ^{1}H NMR spectrum of **3** in $CDCl_3$.

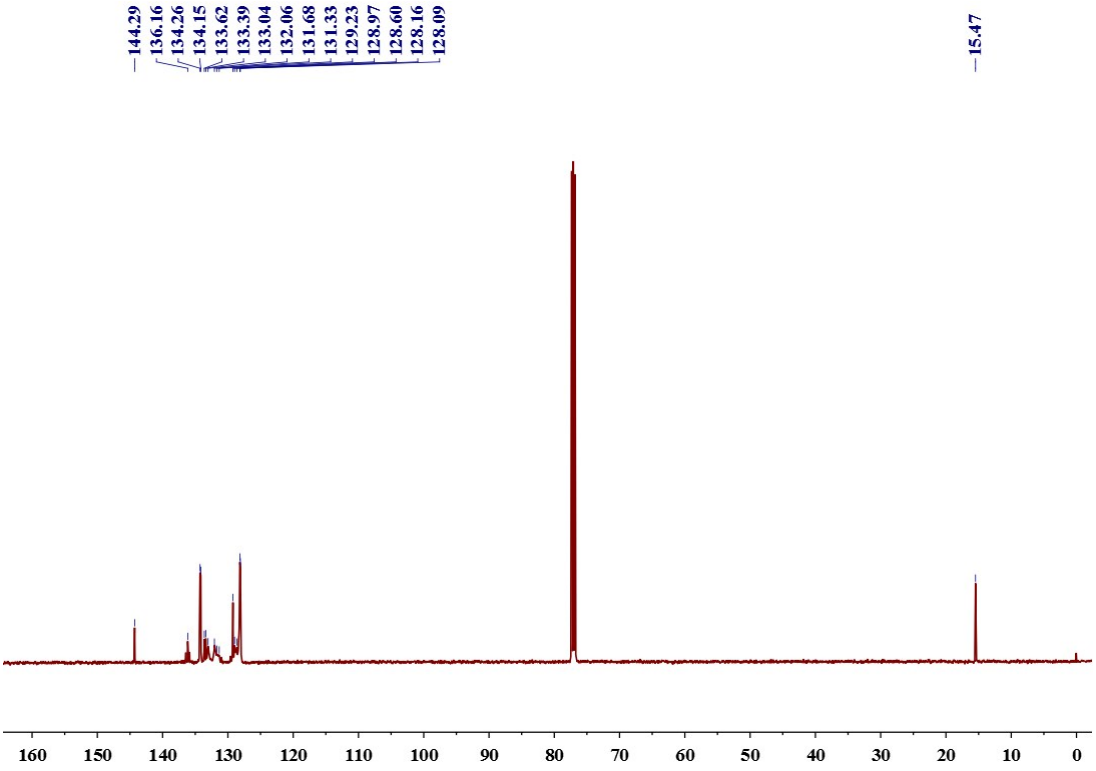

Fig. S7. ^{13}C NMR spectrum of **1** in $CDCl_3$.

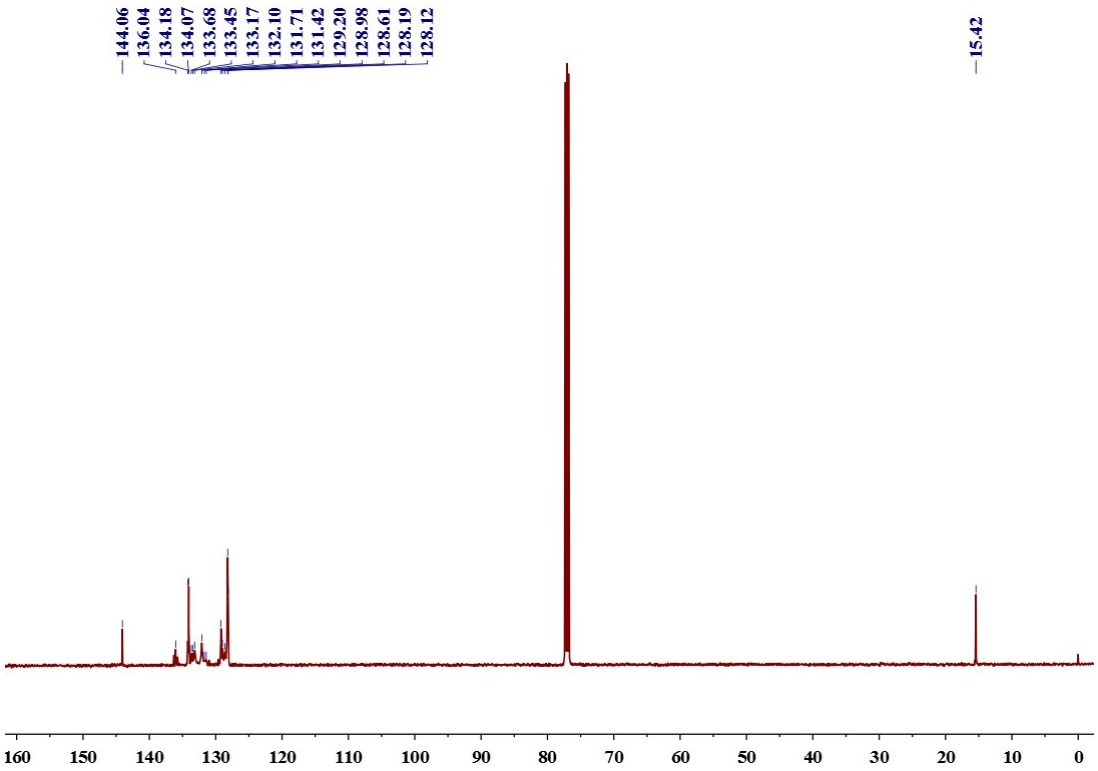

Fig. S8. ^{13}C NMR spectrum of **2** in $CDCl_3$.

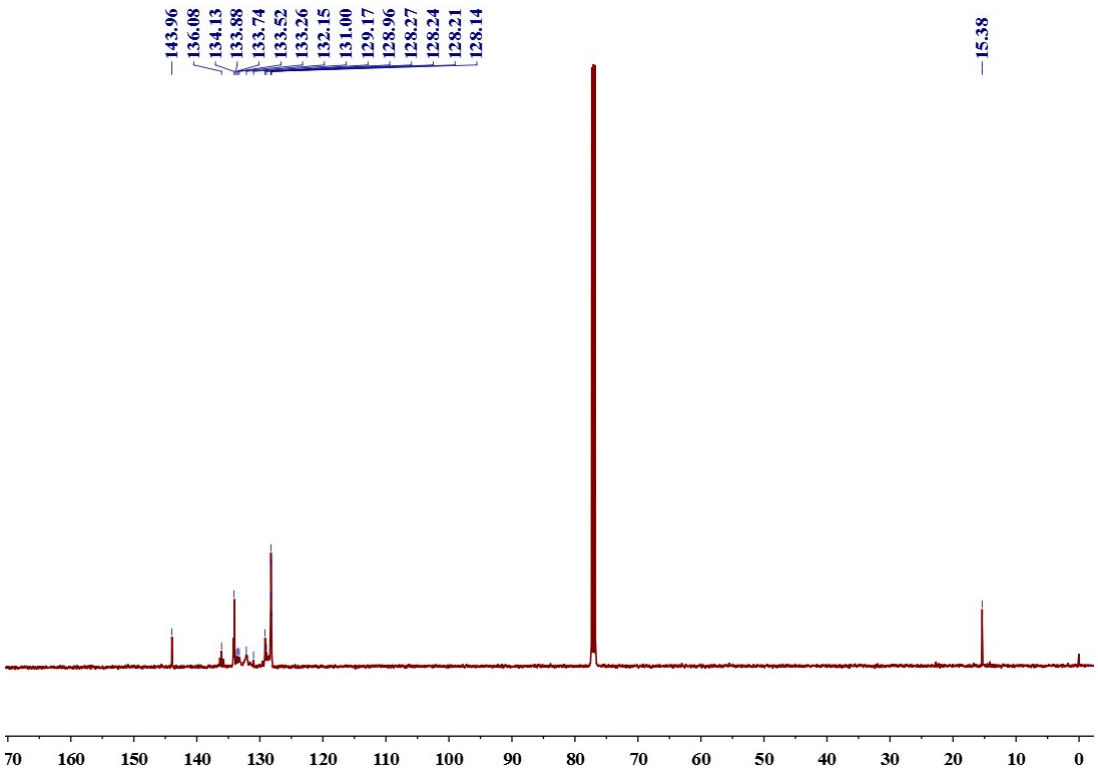

Fig. S9. ^{13}C NMR spectrum of **3** in $CDCl_3$.

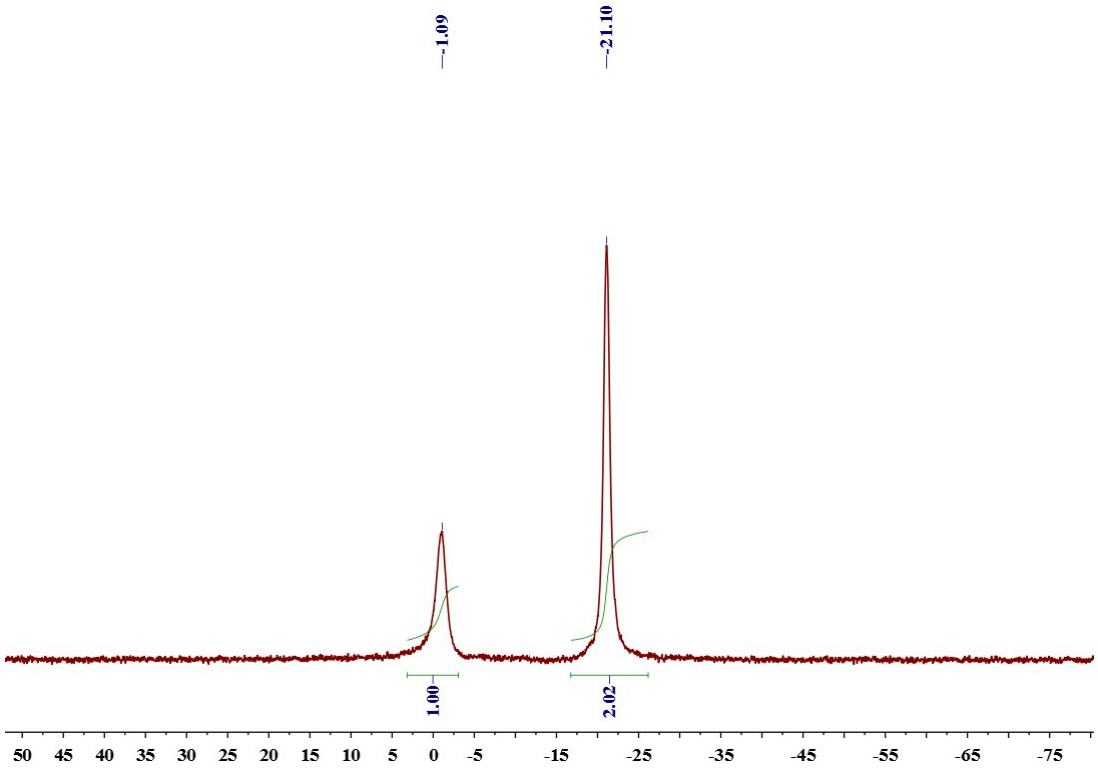

Fig. S10. ^{31}P NMR spectrum of **1** in $CDCl_3$.

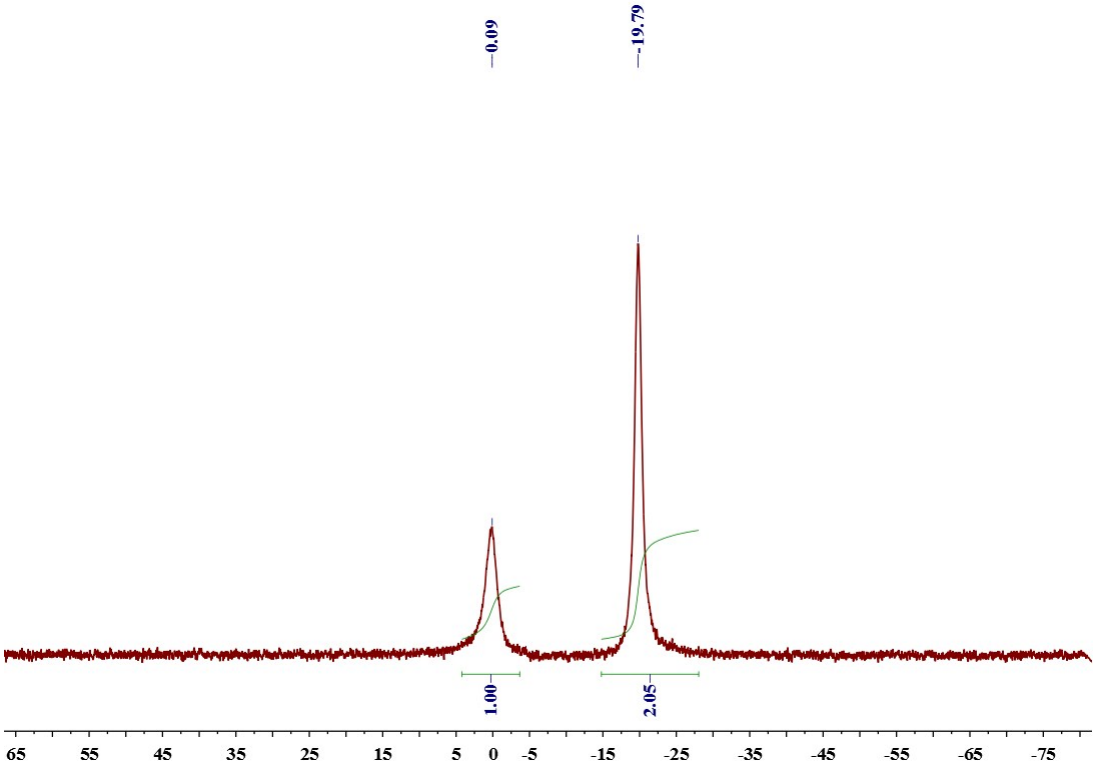

Fig. S11. ^{31}P NMR spectrum of **2** in $CDCl_3$.

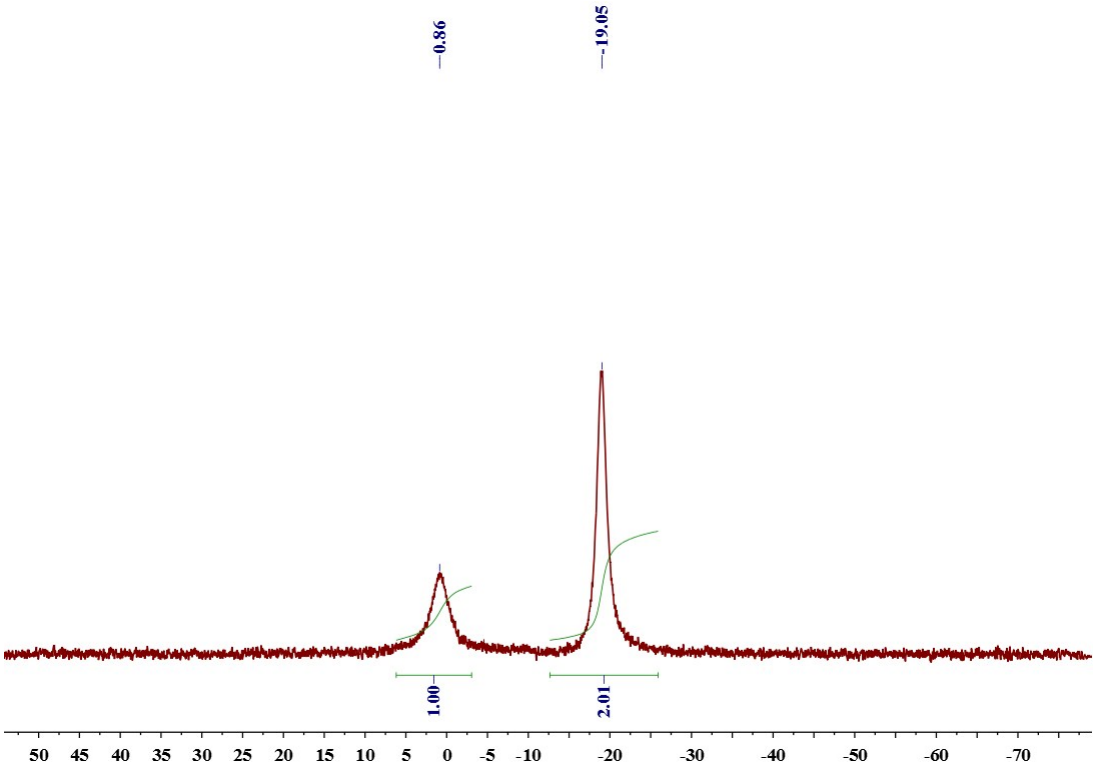

Fig. S12. ^{31}P NMR spectrum of **3** in $CDCl_3$.

2. Molecular structures

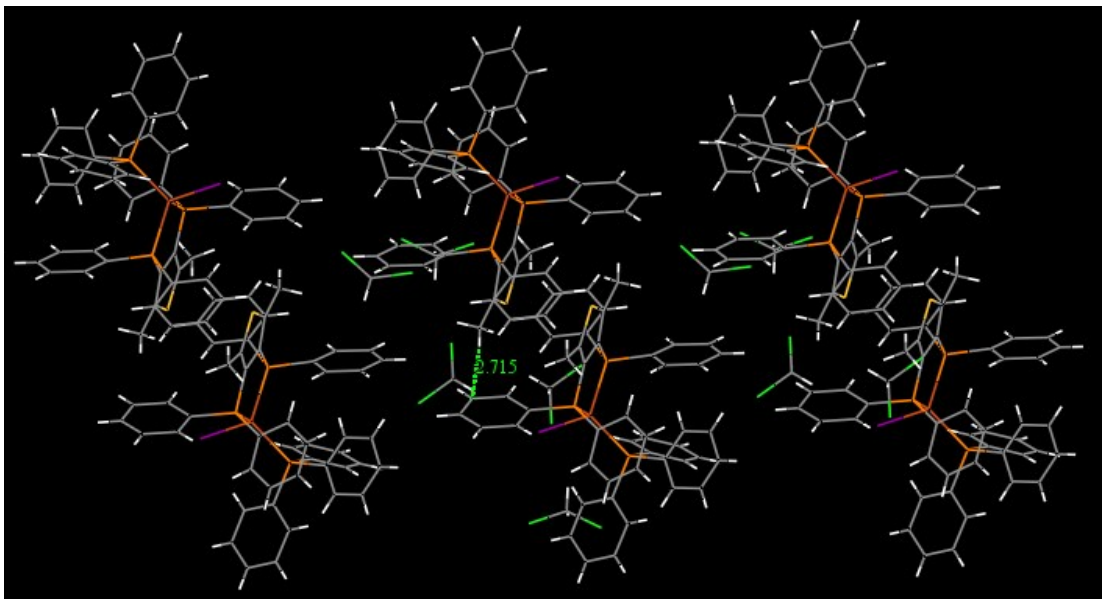

Fig. S13. 1-D molecular structure and C–H···π interactions in **1**.

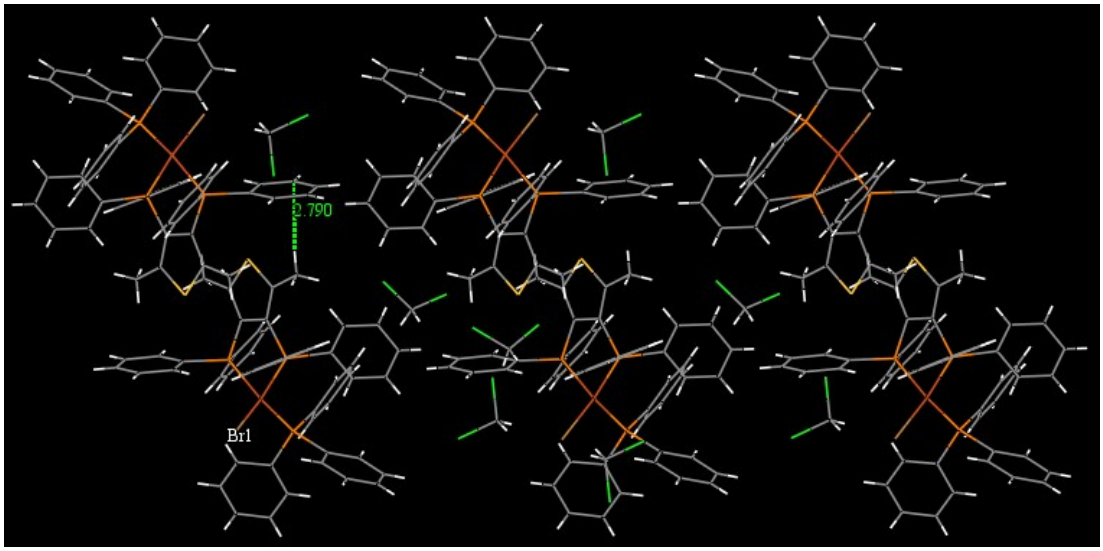

Fig. S14. 1-D molecular structure and C–H···π interactions in **2**.

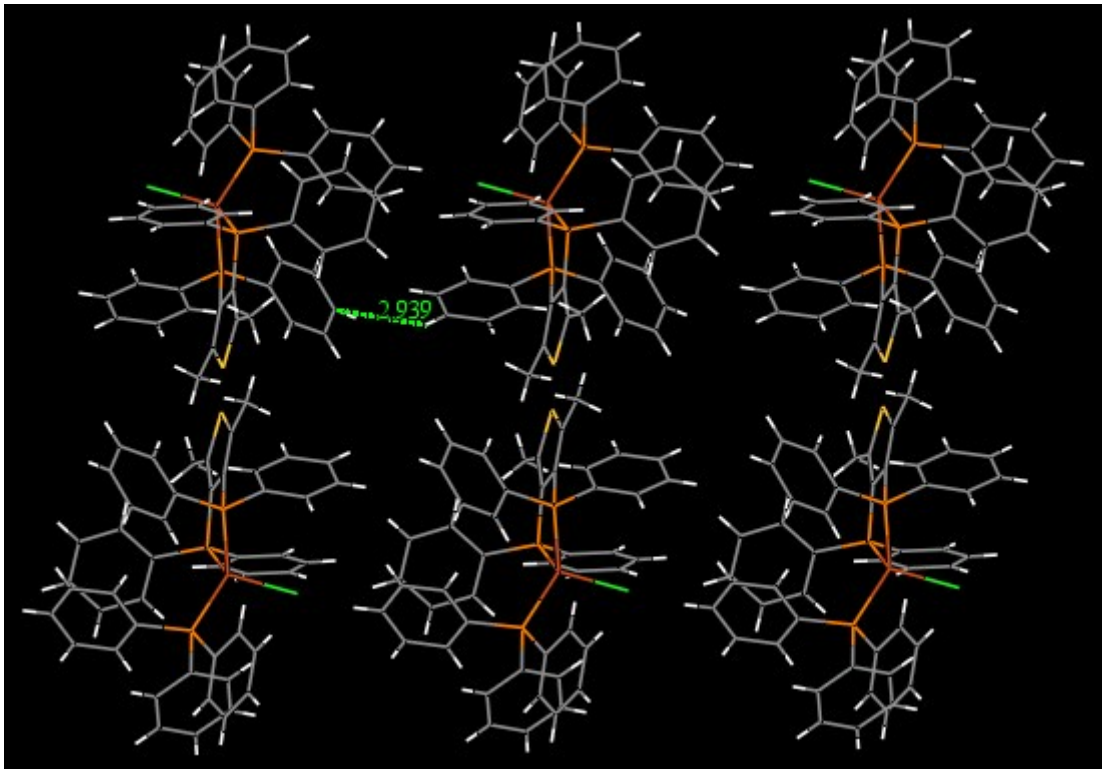

Fig. S15. 1-D molecular structure and C–H···π interactions in **3**.

3. Photophysical properties

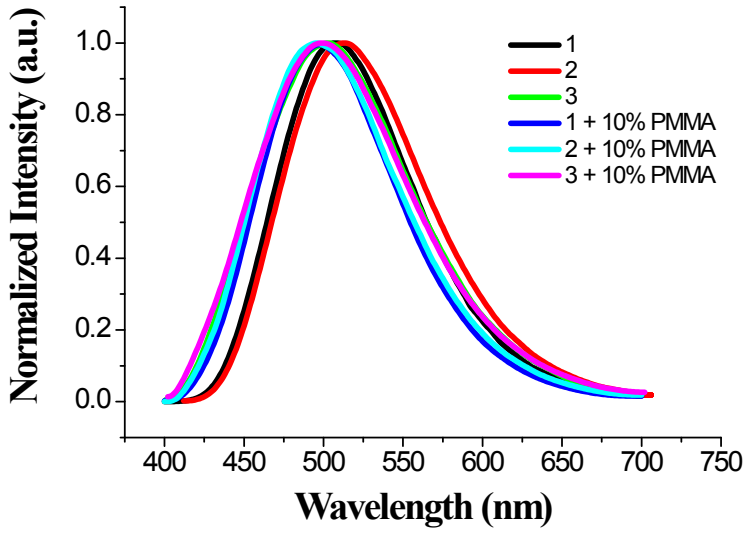

Fig. S16. PL spectra of **1-3** in pristine and in 10% PMMA films.

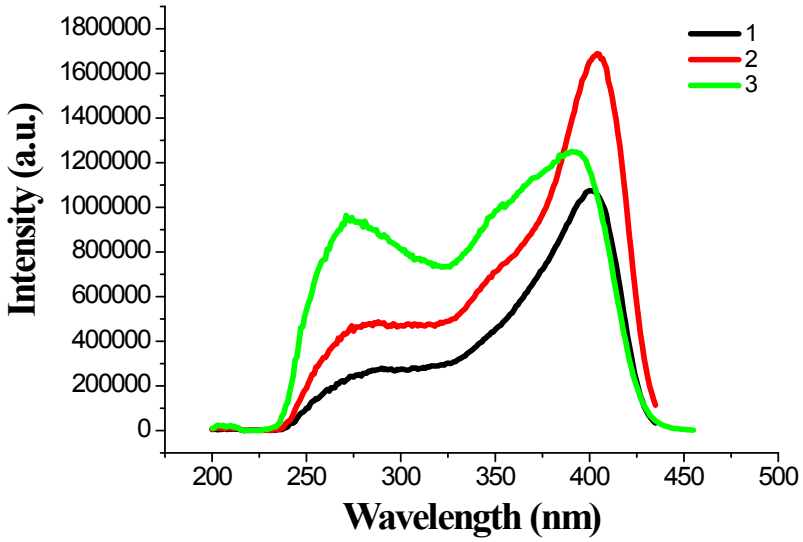

Fig. S17. Excitation spectra of **1-3** in crystal state.

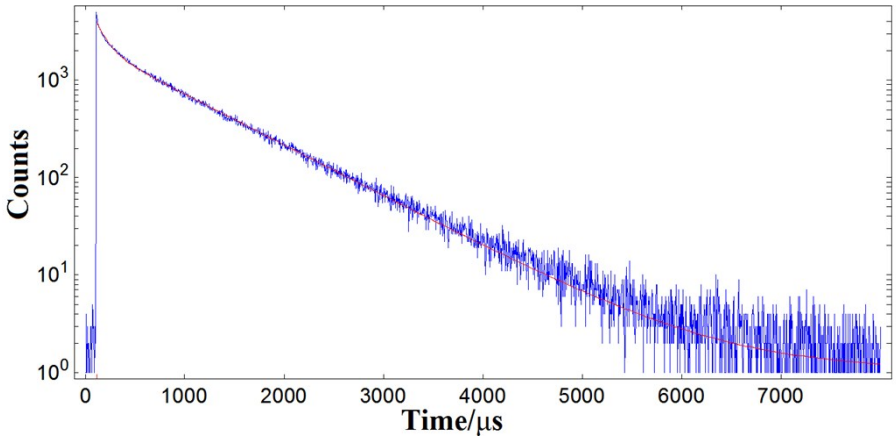

	Fix	Value / μs	Std. Dev / μs		Fix	Value	Std. Dev	Rel %
τ_1	☐	108.3728	1.96519	B_1	☐	1944.482	23.0396	10.78
τ_2	☐	829.7635	1.94095	B_2	☐	2101.846	8.5649	89.22
τ_3	☐			B_3	☐			
τ_4	☐			B_4	☐			
				A	☐	1.070		

χ^2 : 1.195

(in crystal state)

	Fix	Value / μs	Std. Dev / μs		Fix	Value	Std. Dev	Rel %
τ_1	☐	1.2854	0.06805	B_1	☐	0.896	0.0282	2.57
τ_2	☐	20.7018	0.17214	B_2	☐	0.880	0.0092	40.61
τ_3	☐	620.2981	3.47783	B_3	☐	0.041	0.0003	56.82
τ_4	☐			B_4	☐			
δt	☐	0.0002	0.0004	A	☐	-0.014		

χ^2 : 1.103

(in powder state)

Fig. S18. Time profiles of luminescence decay and exponential fit spectrum of **1** at r.t.

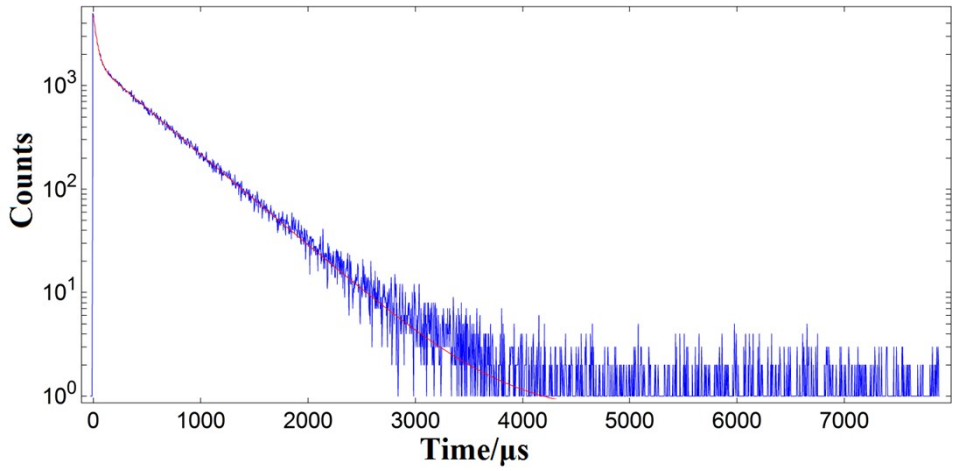

	Fix	Value / μs	Std. Dev / μs		Fix	Value	Std. Dev	Rel %
τ_1	☐	33.7363	0.54892	B_1	☐	3607.876	48.0266	12.85
τ_2	☐	490.8053	1.33990	B_2	☐	1681.683	7.2950	87.15
τ_3	☐			B_3	☐			
τ_4	☐			B_4	☐			
				A	☐	0.675		

χ^2 : 0.852

(in crystal state)

	Value	Std. Dev.		Value	Std. Dev.	Rel. %
τ_1 (s)	3.280E-5	3.303E-7	B1	1.846E+3	1.464E+1	30.66
τ_2 (s)	2.864E-4	1.252E-6	B2	4.781E+2	3.441E+0	69.34
τ_3 (s)	--	--	B3	--	--	--
τ_4 (s)	--	--	B4	--	--	--
χ^2	1.175E+0		A	8.130E-1		

(in powder state)

Fig. S19. Time profiles of luminescence decay and exponential fit spectrum of **2** at r.t.

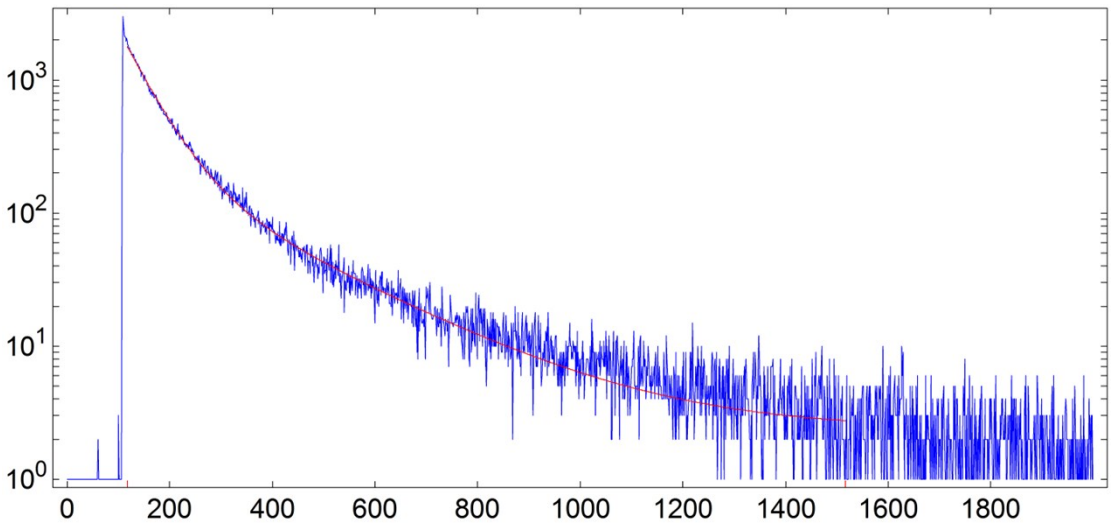

Fit = A + B1.exp(-t/T1) + B2.exp(-t/T2)

	Value	Std Dev		Value	Std Dev	Rel %
T1	5.471E-5	5.562E-7	B1	1.593E+3	1.022E+1	63.89
T2	2.188E-4	3.903E-6	B2	2.252E+2	7.819E+0	36.11
Chisq	1.253E+0		A	2.383E+0		

(in crystal state)

	Fix	Value / µs	Std. Dev / µs		Fix	Value	Std. Dev	Rel %
τ_1	☐	41.3663	0.33010	B_1	☐	1649.567	8.5492	52.06
τ_2	☐	175.2454	1.24378	B_2	☐	358.633	5.4763	47.94
τ_3	☐			B_3	☐			
τ_4	☐			B_4	☐			
				A	☐	1.653		

χ^2 : 1.310

(in powder state)

Fig. S20. Time profiles of luminescence decay and exponential fit spectrum of **3** at r.t.

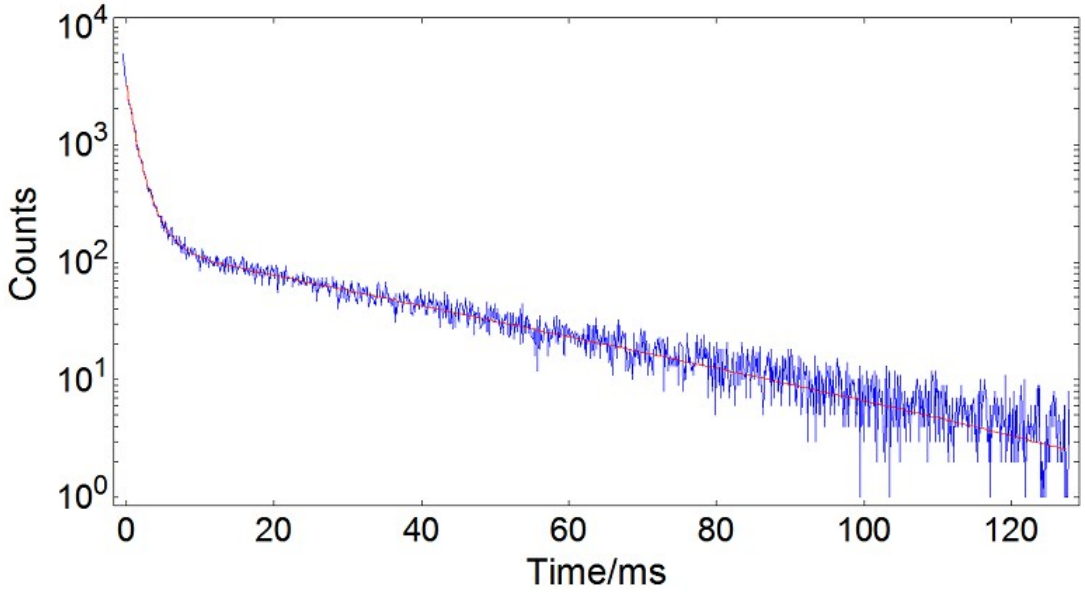

	Fix	Value / ms	Std. Dev / ms		Fix	Value	Std. Dev	Rel %
τ_1	☐	0.7806	0.06293	B_1	☐	2124.569	209.6010	18.48
τ_2	☐	1.8595	0.11175	B_2	☐	1358.792	229.2201	28.16
τ_3	☐	33.8564	0.52339	B_3	☐	141.437	1.7820	53.36
τ_4	☐			B_4	☐			
				A	☐	-0.720		

χ^2 : 1.187

(in crystal state)

	Fix	Value / μs	Std. Dev / μs		Fix	Value	Std. Dev	Rel %
τ_1	☐	1134.7823	21.13242	B_1	☐	237.795	4.0882	36.49
τ_2	☐	17818.8948	341.40864	B_2	☐	26.355	0.4888	63.51
τ_3	☐			B_3	☐			
τ_4	☐			B_4	☐			
				A	☐	0.836		

χ^2 : 1.157

(in powder state)

Fig. S21. Time profiles of luminescence decay and exponential fit spectrum of **1** at 77 K.

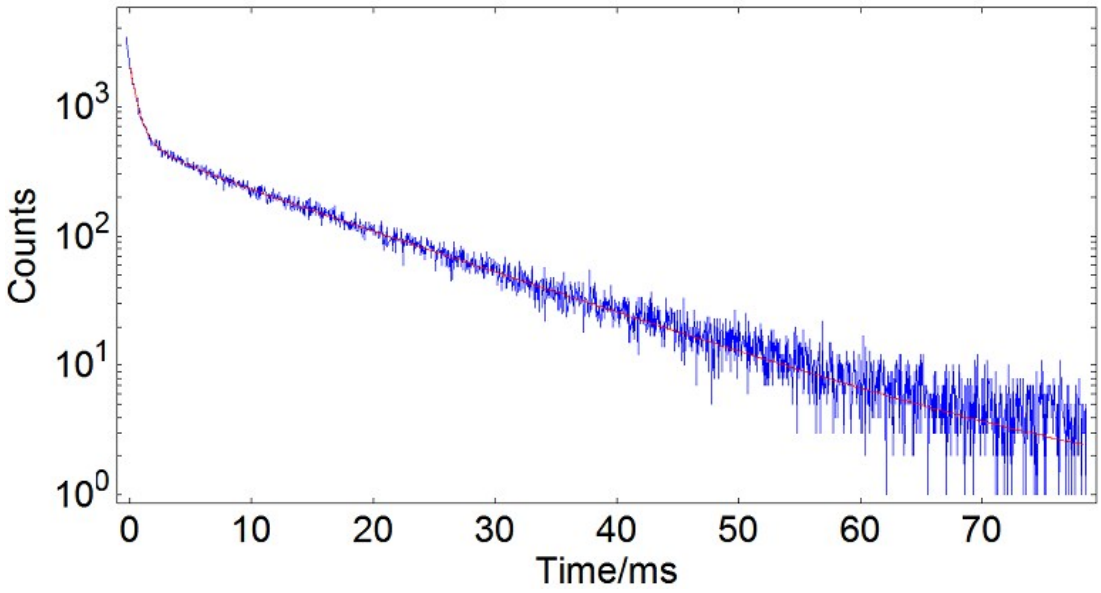

	Fix	Value / μs	Std. Dev / μs		Fix	Value	Std. Dev	Rel %
τ_1	☐	569.9055	20.04261	B_1	☐	1536.784	31.6114	11.40
τ_2	☐	2723.9621	498.89538	B_2	☐	150.036	28.3498	5.32
τ_3	☐	13662.3926	115.18675	B_3	☐	468.347	6.9051	83.28
τ_4	☐			B_4	☐			
				A	☐	0.941		

χ^2 : 1.219

(in crystal state)

	Fix	Value / μs	Std. Dev / μs		Fix	Value	Std. Dev	Rel %
τ_1	☐	1320.4668	24.72782	B_1	☐	988.741	12.1391	8.55
τ_2	☐	11194.9288	24.49107	B_2	☐	1246.700	4.4162	91.45
τ_3	☐			B_3	☐			
τ_4	☐			B_4	☐			
				A	☐	1.938		

χ^2 : 1.416

(in powder state)

Fig. S22. Time profiles of luminescence decay and exponential fit spectrum of **2** at 77 K.

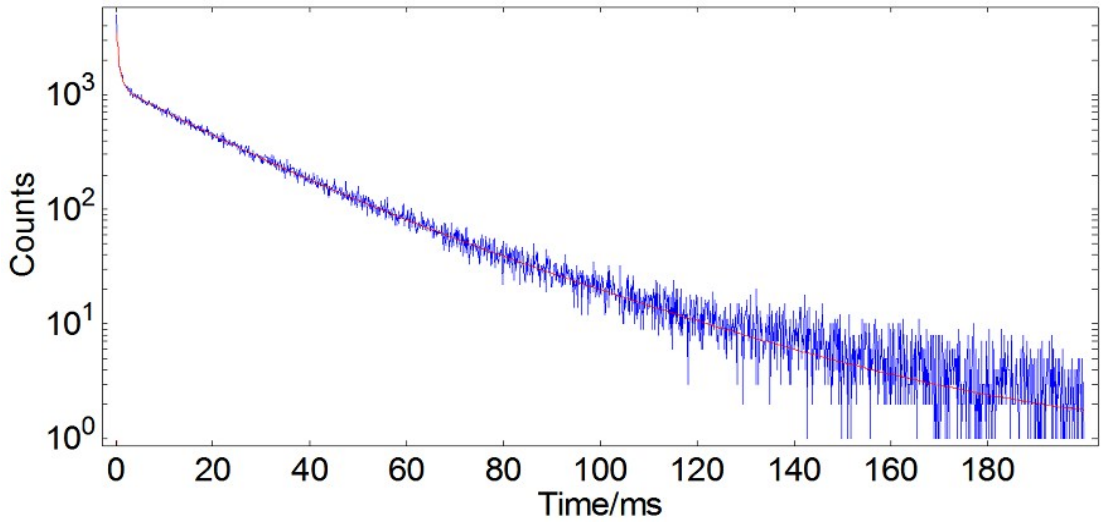

Fit = A + B1.exp(-t/T1) + B2.exp(-t/T2) + B3.exp(-t/T3)

	Value	Std Dev		Value	Std Dev	Rel %
T1	5.969E-4	1.416E-5	B1	2.639E+3	5.133E+1	5.80
T2	1.576E-2	6.124E-4	B2	7.684E+2	5.011E+1	44.58
T3	3.120E-2	1.090E-3	B3	4.321E+2	5.418E+1	49.62
	Chisq	1.249E+0		A	1.047E+0	

(in crystal state)

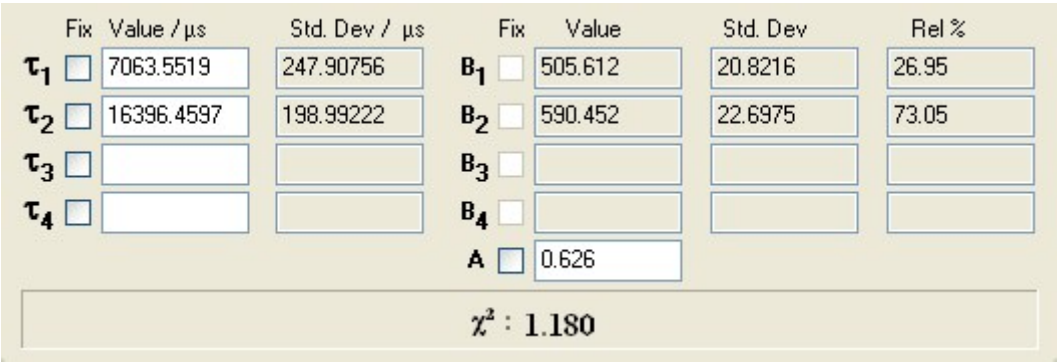

(in powder state)

Fig. S23. Time profiles of luminescence decay and exponential fit spectrum of **3** at 77 K.

4. Computational details

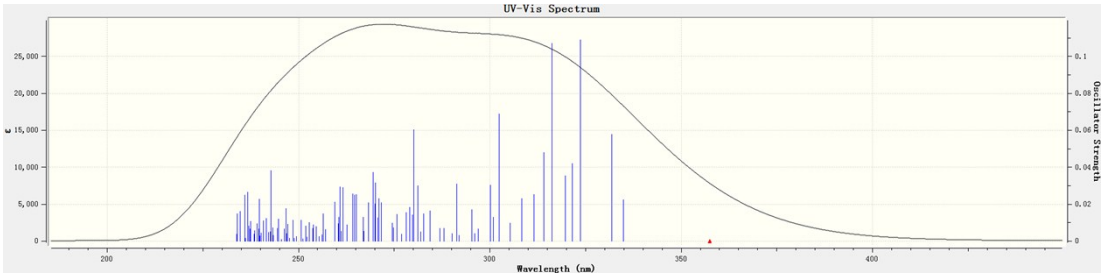

Fig. S24. The absorption spectrum of complex **1** in CH_2Cl_2.

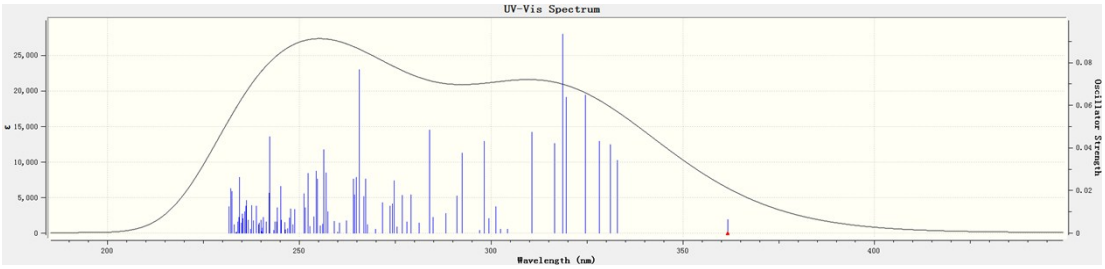

Fig. S25. The absorption spectrum of complex **2** in CH_2Cl_2.

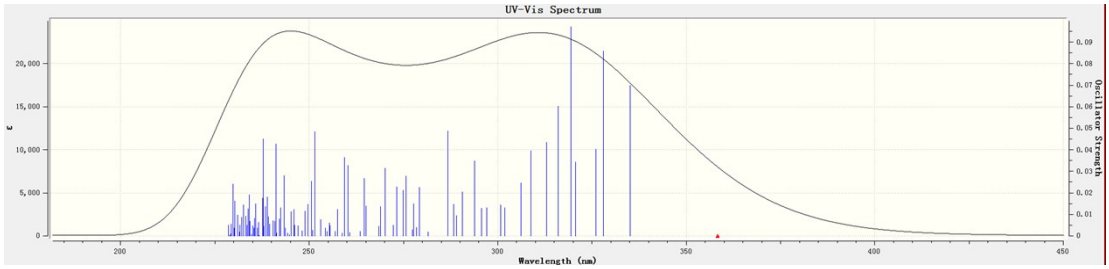

Fig. S26. The absorption spectrum of complex **3** in CH_2Cl_2.

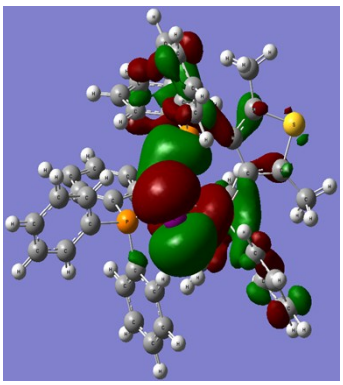

HOMO

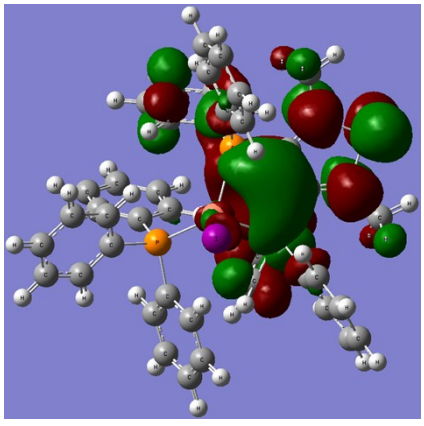

LUMO

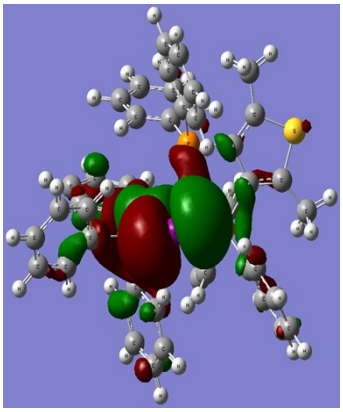

HOMO−1

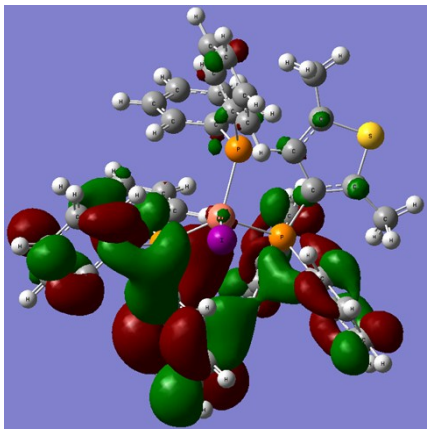

LUMO+1

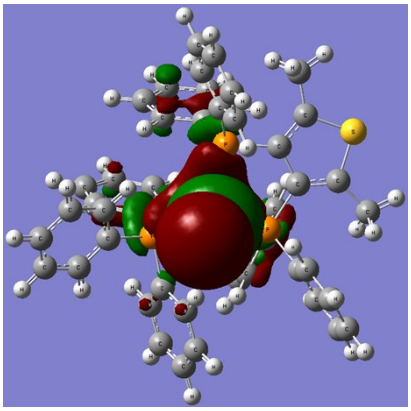

HOMO−2

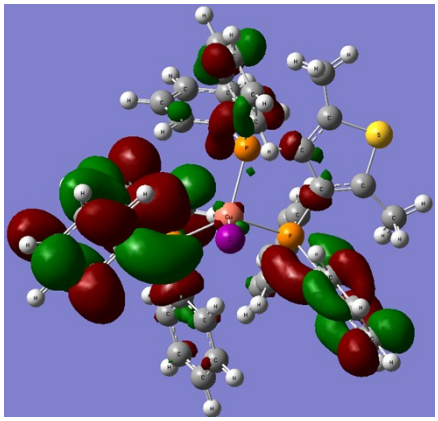

LUMO+2

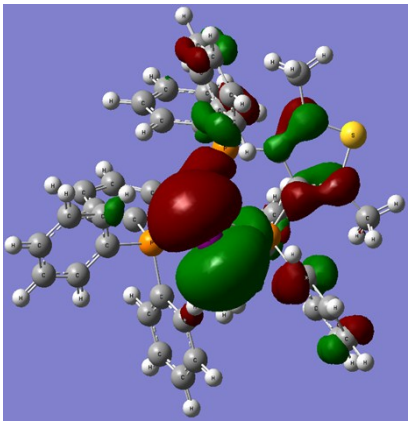

HOMO−3

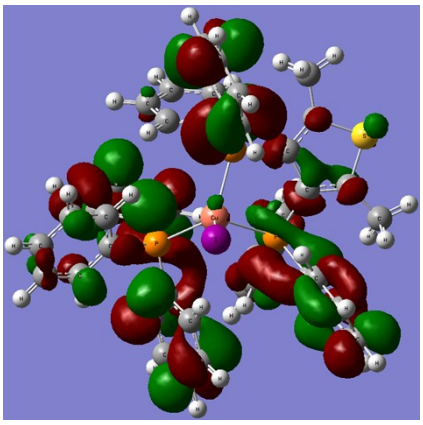

LUMO+3

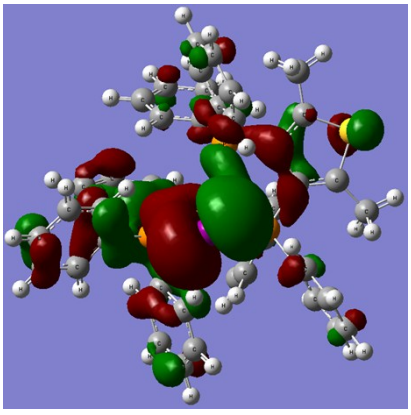

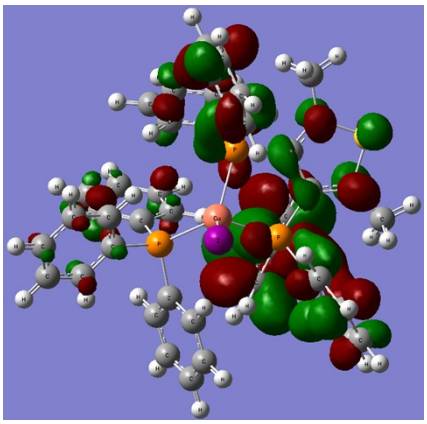

HOMO–4

LUMO+4

1

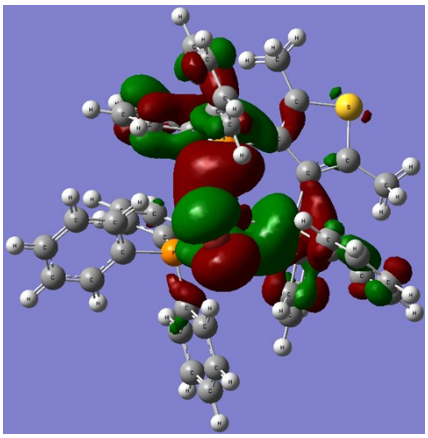

HOMO

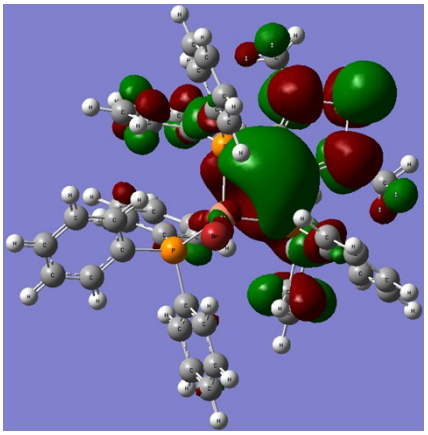

LUMO

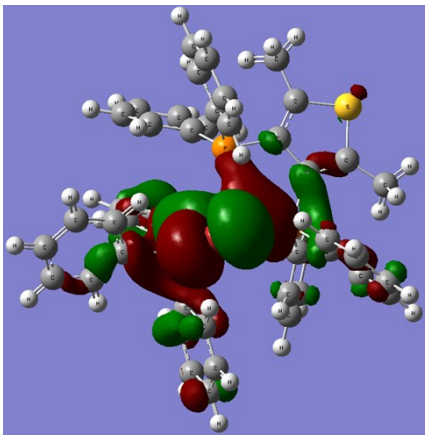

HOMO–1

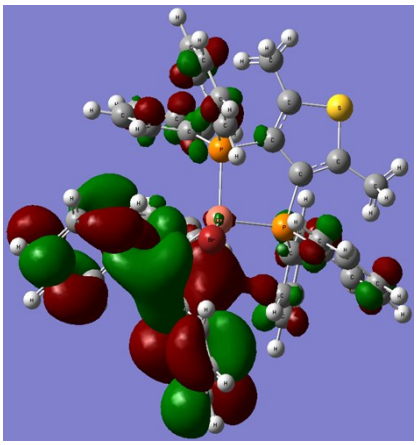

LUMO+1

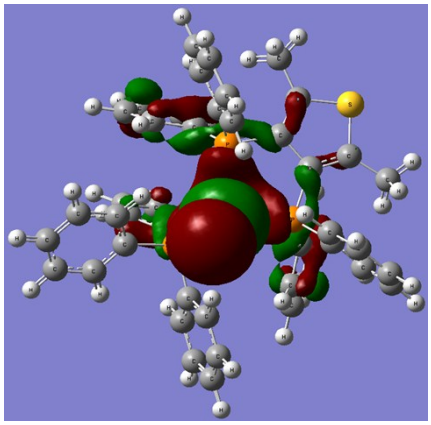

HOMO–2

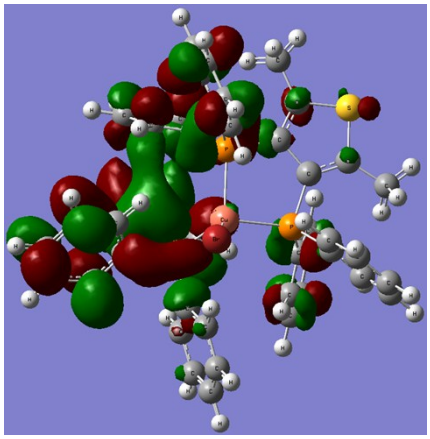

LUMO+2

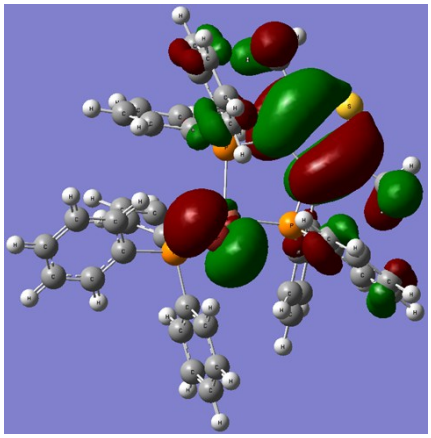

HOMO–3

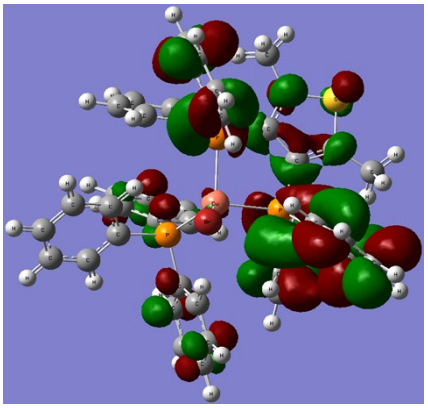

LUMO+3

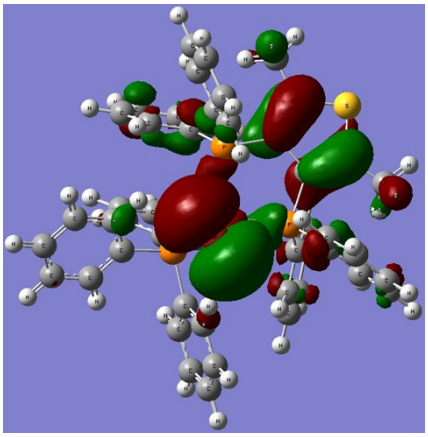

HOMO–4

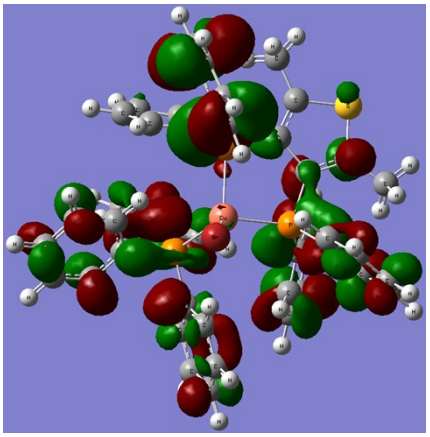

LUMO+4

2

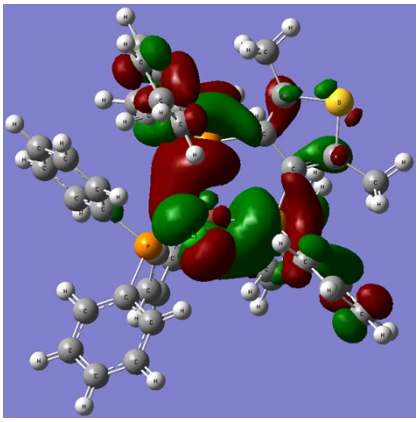

HOMO

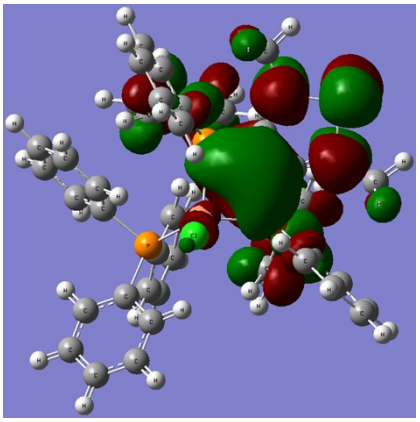

LUMO

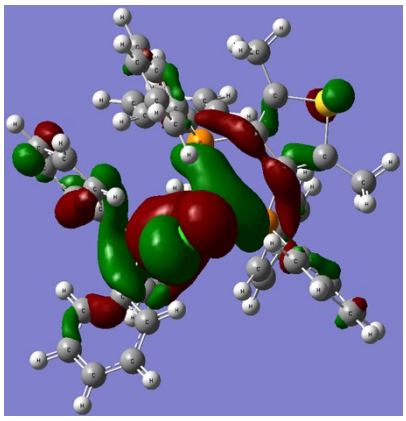

HOMO−1

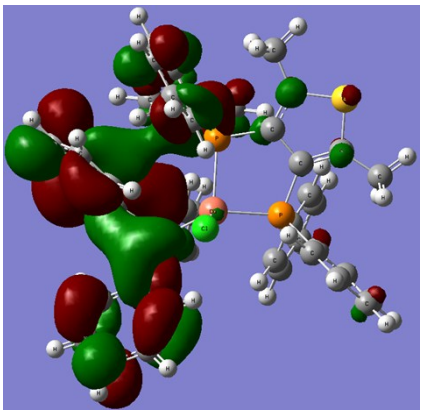

LUMO+1

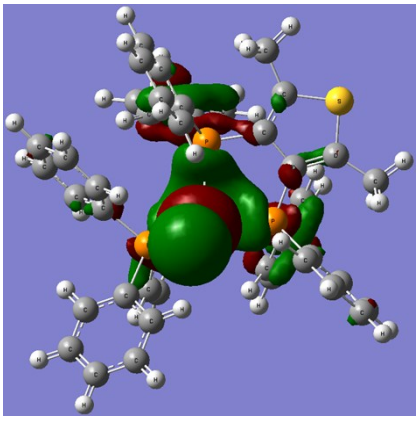

HOMO−2

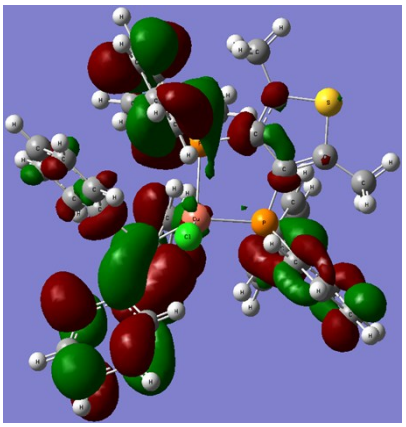

LUMO+2

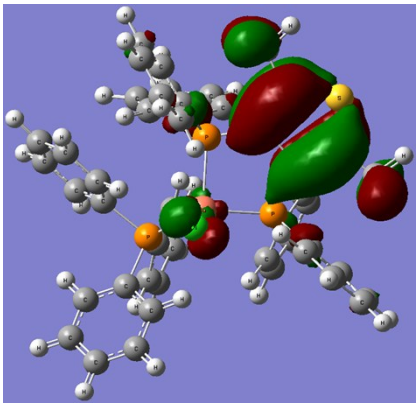

HOMO−3

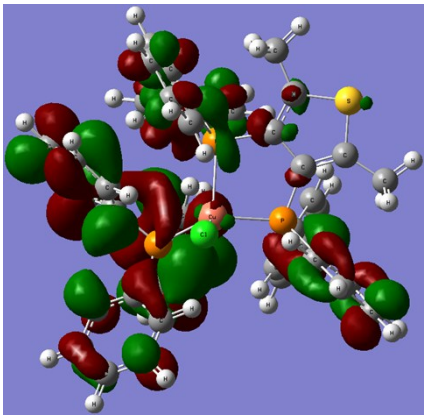

LUMO+3

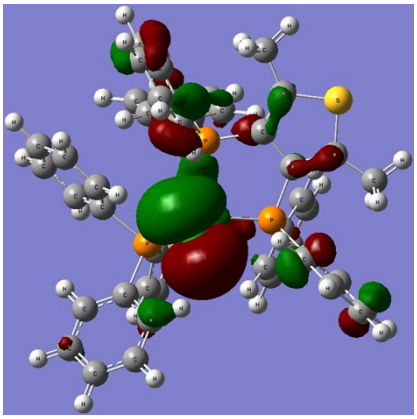

HOMO−4

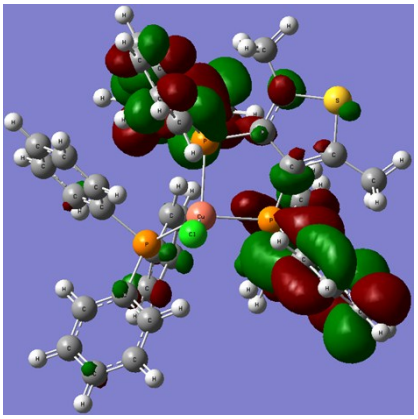

LUMO+4

3

Fig. S27. Contour plots of frontier molecular orbitals of complexes **1–3** in CH_2Cl_2.

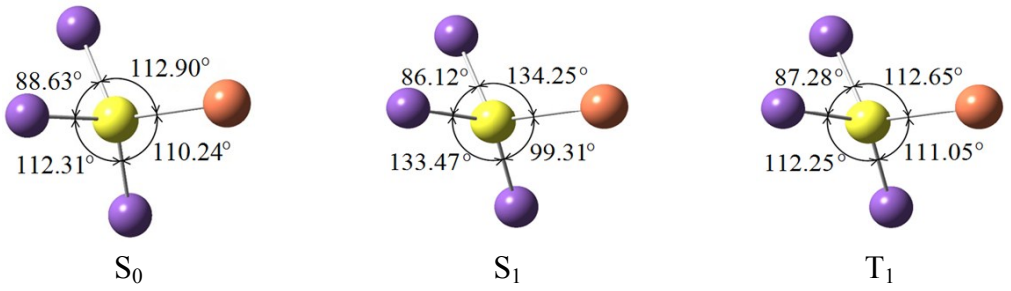

S_0 S_1 T_1

1

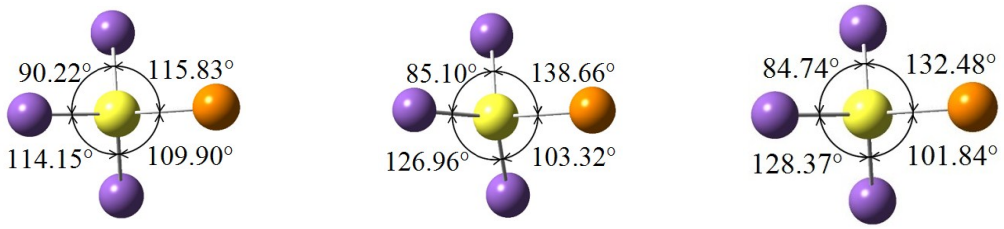

S_0 S_1 T_1

2

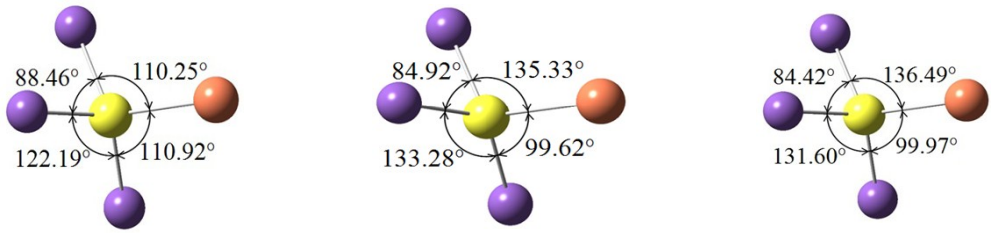

S_0 S_1 T_1

3

Fig. S28. The core structures in the optimized S_0, S_1, and T_1 geometries for complexes **1-3**.

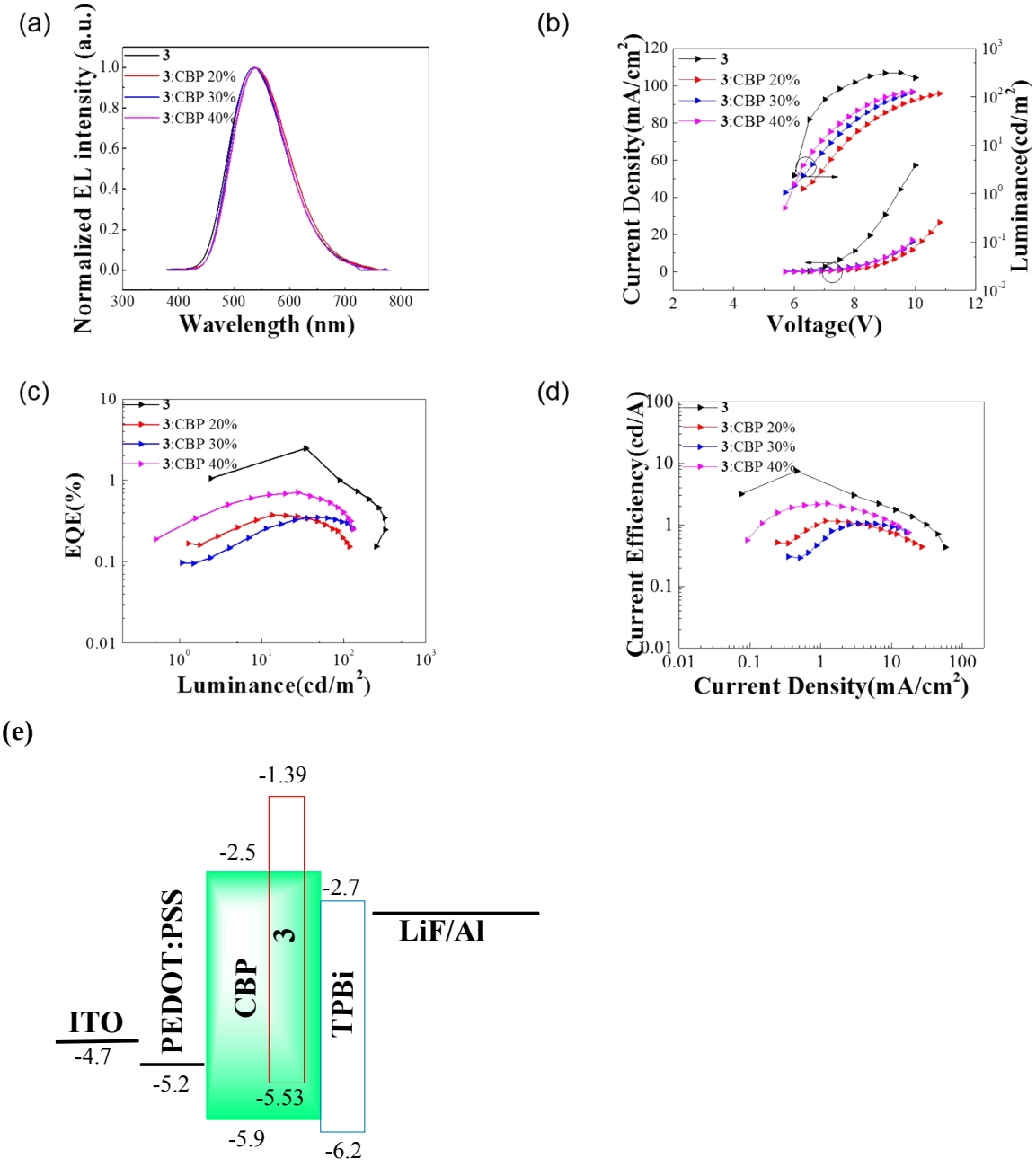

Fig. S29. (a) EL spectra; (b) Current density–voltage–luminance (J–V–L) characteristics; (c) EQE–luminance characteristics; (d) Current efficiency- current density characteristics of the undoped device and doped device with dosage concentration of 20%, 30%, 40% when CBP (1,3-bis(9-carbazolyl)benzene) served as host material; (e) Energy-level diagram of the devices based on the complex **3**.

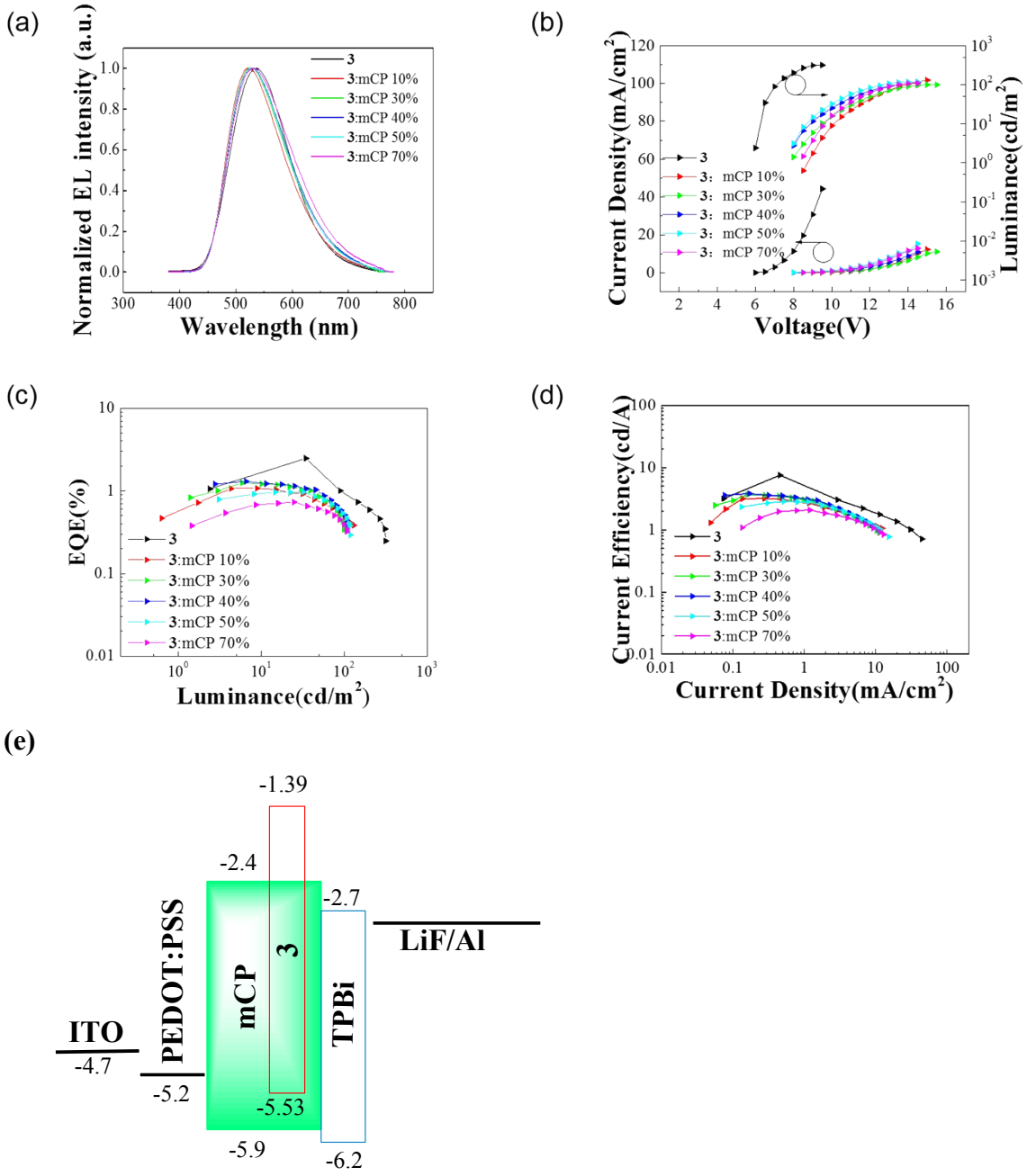

Fig. S30. (a) EL spectra (b) Current density–voltage–luminance (J–V–L) characteristics; (c) EQE–luminance characteristics; (d) Current efficiency- current density characteristics of the undoped device and doped device with dosage concentration of 10%, 30%, 40%, 50%, 70% when mCP (4,4'-Bis(9H-carbazol-9-yl)biphenyl) served as host material; (e) Energy-level diagram of the devices based on the complex **3**.

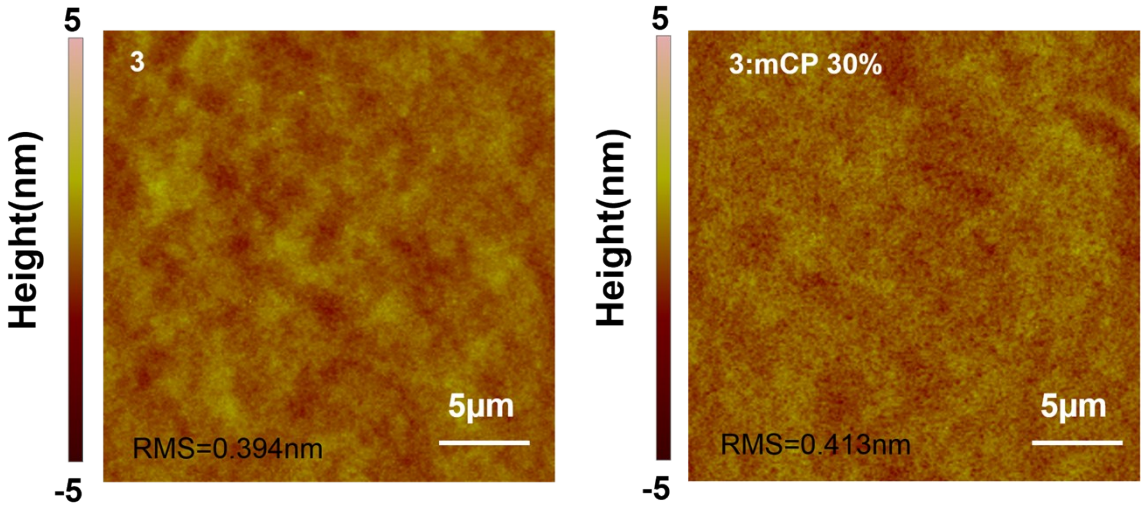

Fig. S31. Atomic force microscopy (AFM) images of the undoped film of complex 2 and the doped film with dosage concentration of 30% when mCP served as host material based on the structure of ITO/PEDOT:PSS/EML.

The doped EML film was prepared by mixing the host material solution (dissolved in chlorobenzene, 15 mg/mL) and complex **3** (dissolved in chlorobenzene, 15 mg/mL) at different volume ratios. The mixture was spin coated onto the substrates at 3000 r.p.m for 50 s and baked at 70 °C for 10 min in the glove box. Except for the EML layer, the rest was the same as that for the undoped device.

Table S1. Selected bond lengths (Å) and angles (°) in the optimized S_0, S_1, and T_1 geometries for complexes **1-3**

Complex	Geometry	Cu-X	Cu-P	P-Cu-P	P-Cu-X
1	S_0	2.6261	2.3754, 2.3280, 2.3054	88.63, 112.31, 119.45	111.62, 112.90, 110.24
	S_1	2.6246	2.3212, 2.3557, 2.3464	86.12, 133.47, 108.92	99.99, 134.25, 99.31
	T_1	2.6234	2.3808, 2.3265, 2.3034	87.28, 112.25, 120.40	110.94, 112.65, 111.05
2	S_0	2.4429	2.3460, 2.3334, 2.3169	90.22, 114.15, 112.47	113.20, 115.83, 109.90
	S_1	2.4084	2.3184, 2.3326,	85.10, 126.96,	100.28, 138.66,

			2.3701	105.67	103.32
	T_1	2.4134	2.31319, 2.33258,	84.74, 128.37,	103.95, 132.48,
			2.36879	108.65	101.84
3	S_0	2.3249	2.29623, 2.31557,	88.46, 122.19,	111.78, 110.25,
			2.38149	110.90	110.92
	S_1	2.2783	2.37675, 2.32155,	84.92, 133.28,	101.88, 135.33,
			2.36089	107.30	99.62
	T_1	2.2798	2.38263, 2.31687,	84.42, 131.60,	103.32, 136.49,
			2.34531	106.28	99.97

Table S2. Energy and compositions of frontiers molecular orbitals of complex **1** in CH_2Cl_2.

MO	Energy(ev)	Cu	I	Thienyl ring	P in dpmt	Phenyl rings in dpmt	P in PPh_3	Phenyl rings in PPh_3
H-4	-6.39	0.04	0.02	0.11	0.13	0.20	0.10	0.40
H-3	-6.20	0.02	0.01	0.07	0.11	0.61	0.01	0.17
H-2	-6.08	0.23	0.01	0.02	0.12	0.21	0.12	0.30
H-1	-5.69	0.13	0.02	0.06	0.08	0.09	0.30	0.32
H	-5.54	0.02	0.01	0.09	0.26	0.45	0.01	0.16
L	-1.38	0.02	0.00	0.08	0.13	0.39	0.09	0.29
L+1	-1.21	0.02	0.00	0.04	0.13	0.32	0.08	0.40
L+2	-1.11	0.01	0.00	0.05	0.03	0.30	0.08	0.53
L+3	-1.08	0.01	0.00	0.15	0.16	0.25	0.08	0.34
L+4	-1.02	0.02	0.00	0.06	0.05	0.79	0.02	0.05

Table S3. Energy and compositions of frontiers molecular orbitals of complex **2** in CH_2Cl_2.

MO	Energy(ev)	Cu	Br	Thienyl ring	P in dpmt	Phenyl rings in dpmt	P in PPh_3	Phenyl rings in PPh_3
H-4	-6.59	0.01	0.02	0.10	0.38	0.35	0.01	0.13
H-3	-6.44	0.02	0.01	0.27	0.05	0.33	0.08	0.24
H-2	-6.26	0.11	0.01	0.05	0.10	0.33	0.08	0.31
H-1	-5.77	0.06	0.01	0.06	0.10	0.16	0.18	0.43
H	-5.53	0.02	0.00	0.07	0.26	0.34	0.03	0.27
L	-1.39	0.02	0.00	0.08	0.07	0.60	0.11	0.12
L+1	-1.19	0.02	0.00	0.07	0.12	0.33	0.09	0.37

L+2	-1.15	0.01	0.00	0.10	0.09	0.31	0.07	0.43
L+3	-1.09	0.02	0.00	0.19	0.10	0.46	0.09	0.14
L+4	-1.03	0.01	0.00	0.18	0.03	0.59	0.05	0.15

Table S4. Energy and compositions of frontiers molecular orbitals of complex **3** in CH_2Cl_2.

MO	Energy(ev)	Cu	Cl	Thienyl ring	P in dpmt	Phenyl rings in dpmt	P in PPh_3	Phenyl rings in PPh_3
H-4	-6.84	0.02	0.02	0.08	0.14	0.54	0.01	0.20
H-3	-6.48	0.01	0.00	0.16	0.21	0.43	0.03	0.18
H-2	-6.31	0.07	0.01	0.04	0.16	0.49	0.03	0.19
H-1	-5.81	0.04	0.01	0.16	0.12	0.19	0.17	0.31
H	-5.53	0.02	0.00	0.08	0.23	0.52	0.01	0.14
L	-1.35	0.01	0.00	0.11	0.07	0.61	0.03	0.17
L+1	-1.22	0.01	0.00	0.05	0.13	0.26	0.09	0.46
L+2	-1.14	0.01	0.00	0.11	0.09	0.31	0.07	0.41
L+3	-1.07	0.01	0.00	0.13	0.08	0.22	0.08	0.49
L+4	-1.03	0.05	0.00	0.12	0.04	0.69	0.01	0.09

Table S5. Computed excitation states for complex **1** in CH_2Cl_2.

State	λ(nm)/*E*(eV)	Configurations	*f*
1	357.4 (3.47)	H→L(98)	0.0002
3	331.9 (3.74)	H→L+1 (91); H→L+2 (4) ; H→L+3 (2)	0.0579
4	323.7 (3.83)	H-1→L+1 (2); H→L+1 (6); H→L+2 (63) ; H→L+3 (25)	0.1089
7	316.2 (3.92)	H-1→L+3 (2); H→L+4 (89)	0.1071
12	302.4 (4.10)	H-2→L (73); H-1→L+3 (2); H-1→L+4 (18)	0.0689
27	280.1 (4.43)	H-4→L (82); H-1→L+9 (3); H→L+11 (4)	0.0604

Table S6. Computed excitation states for complex **2** in CH_2Cl_2.

State	λ(nm)/*E*(eV)	Configurations	*f*
1	361.8 (3.43)	H→L (97)	0.0064
5	324.5 (3.82)	H→L+1 (4); H→L+2 (11); H→L+3 (82)	0.0647
6	319.5 (3.88)	H-1→L+1 (3); H→L+4 (69); H→L+5 (23)	0.0637
7	318.7 (3.89)	H-1→L+1 (2); H→L+4 (19); H→L+5 (74)	0.0933
34	265.6 (4.67)	H-5→L (12); H-2→L+3 (5); H-2→L+5 (52); H-1→L+11 (19)	0.0768

Table S7. Computed excitation states for complex **3** in CH_2Cl_2.

State	λ(nm)/*E*(eV)	Configurations	*f*
1	358.4 (3.46)	H→L(98)	0.0007
2	335.1 (3.70)	H→L+1 (84); H→L+2 (14)	0.0698
3	328.0 (3.78)	H→L+1 (14); H→L+2 (76); H→L+3 (5)	0.0858
6	319.4 (3.88)	H-1→L+1 (4); H→L+2 (3); H→L+3 (11) ; H→L+4 (78)	0.0972
7	316.0 (3.92)	H-1→L (2); H-1→L+1 (83); H-1→L+2 (9) ; H→L+4 (3)	0.0601